Chemical Science

EDGE ARTICLE

View Article Online
View Journal | View Issue

Cite this: *Chem. Sci.*, 2015, **6**, 4690

Insight into the strong aggregation-induced emission of low-conjugated racemic C6-unsubstituted tetrahydropyrimidines through crystal-structure–property relationship of polymorphs†

Qiuhua Zhu,[a] Yilin Zhang,[b] Han Nie,[c] Zujin Zhao,[c] Shuwen Liu,*[a] Kam Sing Wong*[b] and Ben Zhong Tang*[cd]

Racemic C6-unsubstituted tetrahydropyrimidines (THPs) are a series of fluorophores with a strong aggregation-induced emission (AIE) effect. However, they do not possess the structural features of conventional AIE compounds. In order to understand their AIE mechanism, here, the influences of the molecular packing mode and the conformation on the optical properties of THPs were investigated using seven crystalline polymorphs of three THPs (**1–3**). The racemic THPs **1–3** have low-conjugated and highly flexible molecular structures, and hence show practically no emission in different organic solvents. However, the fluorescence quantum yields of their polymorphs are up to 93%, and the maximum excitation (λ_{ex}) and emission (λ_{em}) wavelengths of the polymorphs are long at 409 and 484 nm, respectively. Single-crystal structures and theoretical calculation of the HOMOs and LUMOs based on the molecular conformations of these polymorphs indicate that the polymorphs with the shortest λ_{ex} and λ_{em} values possess a *RS*-packing mode (*R*- and *S*-enantiomers self-assemble as paired anti-parallel lines) and a more twisted conformation without through-space conjugation between the dicarboxylates, but the polymorphs with longer λ_{ex} and λ_{em} values adopt a *RR*/*SS*-packing mode (*R*- and *S*-enantiomers self-assemble as unpaired zigzag lines) and a less twisted conformation with through-space conjugation between the dicarboxylates. The molecular conformations of **1–3** in all these polymorphs are stereo and more twisted than those in solution. Although **1–3** are poorly conjugated, the radiative rate constants (k_r) of their polymorphs are as large as conventional fluorophores (0.41–1.03 × 10^8 s^{-1}) because of improved electronic conjugation by both through-bond and through-space interactions. Based on the obtained results, it can be deduced that the strong AIE arises not only from the restriction of intramolecular motion but also from enhanced electronic coupling and radiatively-favored inter-crossed local excitation (LE) and intramolecular charge transfer (ICT) excitation states. The abnormal molecular structures, easily-controllable self-assembly of the *R*- and *S*-enantiomers, and the strong AIE effect make THPs very useful fluorophores for applications and theoretical research.

Received 6th April 2015
Accepted 26th May 2015

DOI: 10.1039/c5sc01226k

www.rsc.org/chemicalscience

Introduction

Solid organic fluorophores have received considerable attention owing to their practical applications, such as organic light-emitting diodes (OLEDs)[1] and optical waveguides.[2] However, highly emissive organic fluorophores in solution often show weak or even zero emission when aggregated, which has frequently been referred to as the aggregation-caused quenching (ACQ) effect.[3] In 2001, a propeller-like fluorophore, 1-methyl-1,2,3,4,5-pentaphenylsilole, was found to be not emissive in solution but highly emissive in aggregates,[4] which was termed aggregation-induced emission (AIE). During the last decade, AIE compounds have shown great advantages in many application areas such as OLEDs[5] and chemo/biosensors.[6] A

[a]*School of Pharmaceutical Sciences, Southern Medical University, 1838 Guangzhou Avenue North, Guangzhou 510515, China. E-mail: liusw@smu.edu.cn*

[b]*Department of Physics, The Hong Kong University of Science and Technology, Clear Water Bay, Kowloon, Hong Kong. E-mail: phkswong@ust.hk*

[c]*Guangdong Innovative Research Team, State Key Laboratory of Luminescent Materials and Devices, South China University of Technology, Guangzhou 510640, China*

[d]*Department of Chemistry, State Key Laboratory of Molecular Neuroscience, Institute of Molecular Functional Materials, The Hong Kong University of Science and Technology, Clear Water Bay, Kowloon, Hong Kong, China. E-mail: tangbenz@ust.hk*

† Electronic supplementary information (ESI) available: General method, instruments, preparation of polymorphs, characterization data, ^{1}H and ^{13}C NMR of THP **3**, Table S1 and S2, Fig. S1–S4, "cif" files containing single-crystal X-ray diffraction data of **2c**, **2c'**, **3p**, **3b** and **3c**. CCDC 850811, 1011037–1011040. For ESI and crystallographic data in CIF or other electronic format see DOI: 10.1039/c5sc01226k

conjugated moiety with multiple rotatable aryl groups, such as polyarylated ethenes[7,8] and siloles,[4,9] is considered a structural feature of AIE compounds.[10]

We recently developed a five-component reaction (5CR) for the synthesis of C-6 unsubstituted tetrahydropyrimidines (THPs).[11] THPs show practically no emission in solution but strong emission in aggregates with fluorescence quantum yields up to 93%,[11] presenting a strong AIE effect. Unlike other reported small organic AIE compounds, THPs do not have a π-conjugated stator connected to multiple rotatable aryl groups. The structural characteristic of THPs is a non-aromatic chiral central ring (tetrahydropyrimidine) connected with three aryl rings that are not conjugated with each other. In addition to their unusual AIE properties, THPs were found to have an abnormal response to copper(II)[12] and unique properties in surfactant micelles.[13] Since the emission of THPs is attributed to aggregation and as one of the THPs (**1** in Fig. 1) was found to form two fluorescent polymorphs (**1b** and **1c**),[11] we wonder if other THPs could form different fluorescent polymorphs. If so, it might be possible to study the influences of molecular packing and conformation on their optical properties without a change in the molecular structure, another important factor correlating with optical properties. Fortunately, two polymorphs (**2c** and **2c′**) of THP **2** and three polymorphs (**3b**, **3c** and **3p**) of THP **3** (Fig. 1) were obtained. Then, the fluorescence properties and single crystal structures of these polymorphs were investigated. We report our results here.

Results and discussion

Preparation of the polymorphs (1b, 1c, 2c, 2c′, 3b, 3p and 3c) of THPs 1–3

The polymorphs of THPs **1–3** can be prepared by recrystallization from dichloromethane/*n*-hexane (for all polymorphs except **3p**) or ethyl acetate/*n*-hexane (for **3p**) solution under different conditions. Thermodynamic conditions (high temperature, low concentration and long time) are favorable for the formation of polymorphs **1b** and **2c**, but kinetic conditions (low temperature, high concentration and short time) favor the formation of polymorphs **1c** and **2c′**. Polymorphs **3b** and **3c** were prepared by slow recrystallization at 4 °C, and **3p** at room temperature.

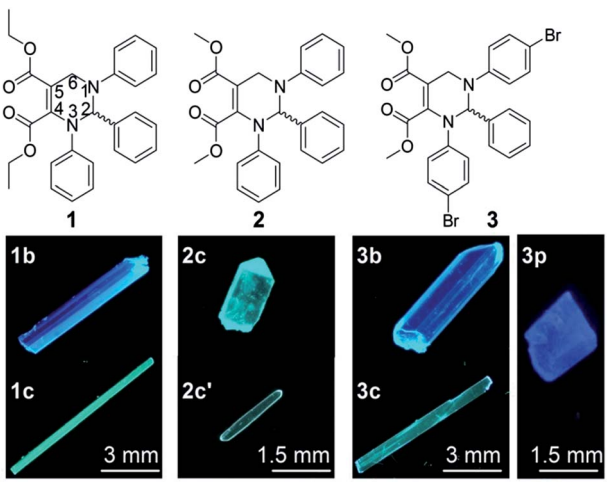

Fig. 1 Molecular structures of the racemic THPs **1–3** and their polymorphs under UV light (350 nm). **1b** and **1c** represent the blue- and cyan-fluorescence polymorphs of **1**; **2c** and **2c′** represent different cyan-fluorescence polymorphs of **2**; **3b**, **3c** and **3p** represent the blue-, cyan- and purple-fluorescence polymorphs of **3**, respectively.

Absorption spectra of THPs 1–3 in solution and the fluorescence properties of their polymorphs

Fig. 2 shows the absorption spectra of THPs **1–3** in solution as well as the excitation and emission spectra of their polymorphs. As depicted in Fig. 2A, the absorption spectrum of **1** is almost the same as that of **2** except it has a slightly higher absorbance. The absorption peaks at lower energy (317 nm) of **1** and **2** are slightly shorter than that (320 nm) of **3**. THPs **1–3** in different organic solvents (cyclohexane, ethanol and acetonitrile *etc.*) are practically non-emissive (insets in Fig. 2A, their emission spectra are lines parallel to the *x*-coordinate), but their crystalline polymorphs are highly emissive (Fig. 1). The excitation and emission spectra of these polymorphs are depicted in Fig. 2B–D. The lower energy peak wavelengths in the excitation spectra of these polymorphs, except for **3p**, show large red shifts (38–92 nm) with respect to the corresponding absorption peaks in Fig. 2A. The peak emission wavelengths (λ_{em}) of these polymorphs vary from 425 to 484 nm (Fig. 2B–D and Table 1), revealing that the molecular packing in different polymorphs has a great impact on the emission wavelengths.

The fluorescence quantum yields (Φ_F) of the polymorphs of **1–3** were determined by a calibrated integrating sphere. The Φ_F values of these polymorphs range from 20 to 93%. The Φ_F values of **1c** and **3c** with longer λ_{em} values are higher than those of their corresponding polymorphs **1b** and **3p** with shorter λ_{em} values. However, for **2c** and **2c′**, **3p** and **3b**, the opposite is the case (Table 1). These results indicate that the Φ_F values are independent of λ_{em} values.

The fluorescence lifetimes (τ) of the polymorphs of **1–3** were measured to understand the nature of the excited state. All the fluorescence decay profiles can be well-fitted by a single exponential decay (Fig. S1†). The τ values of these polymorphs are shown in Table 1. Similar to the quantum yields, the τ values are independent of λ_{em} values.

Since both τ and Φ_F depend on the radiative rate constant (k_r) and the non-radiative rate constant (k_{nr}), that is, $\tau = 1/(k_r + k_{nr})$ and $\Phi_F = k_r/(k_r + k_{nr})$, the k_r ($k_r = \Phi_F/\tau$) and k_{nr} ($k_{nr} = (1 - \Phi_F)/\tau$) values were calculated. As shown in Table 1, the k_r values of these polymorphs are similar ($0.41–1.03 \times 10^8$ s^{-1}) and are inversely proportional to the λ_{em} values of these polymorphs. However, the k_{nr} values are significantly different ($0.05–3.48 \times 10^8$ s^{-1}) and are unrelated to the λ_{em} values.

Molecular stacking modes of the polymorphs of the racemic THPs 1–3

To investigate the influence of enantiomer packing alignments on the fluorescence properties of these polymorphs, their single-crystal structures were determined by X-ray diffraction. Interestingly, all the polymorphs with the shortest

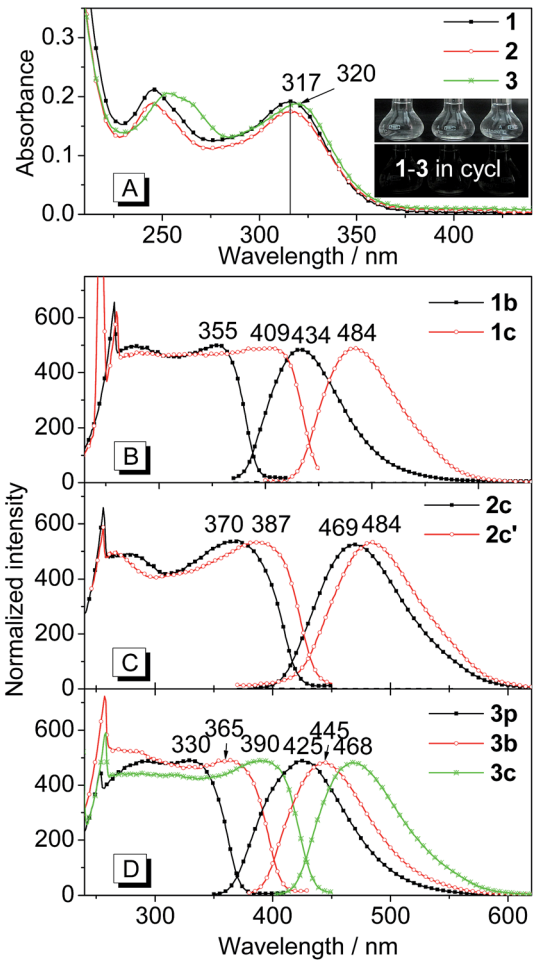

Fig. 2 Optical properties of THPs **1–3**. (A) Absorption spectra of **1–3** in cyclohexane solutions (1.0×10^{-5} M). (B–D) Excitation (left) and emission (right) spectra of the polymorphs of **1–3**, respectively. Excitation and emission spectra were detected by emission and excitation at the peak wavelengths marked in (B–D). Insets in (A) are THPs **1–3** in cyclohexane solutions under daylight (top) and UV light at 365 nm (bottom).

Table 1 Fluorescence properties of the polymorphs of THPs **1–3**

THP	1		2		3		
Polymorph	**1b**	**1c**	**2c**	**2c′**	**3p**	**3b**	**3c**
λ_{ex}[a]/nm	355	409	370	387	330	365	390
λ_{em}[b]/nm	434	484	469	484	425	445	468
Φ_F[c]/%	72	93	48	28	30	20	52
τ[d]/ns	7.1	14	11	6.8	2.9	2.3	7.6
$k_r/s^{-1} \times 10^8$	1.01	0.66	0.44	0.41	1.03	0.87	0.68
$k_{nr}/s^{-1} \times 10^8$	0.39	0.05	0.47	1.06	2.41	3.48	0.63

[a] Peak excitation wavelength at lower energy area. [b] Peak emission wavelength. [c] Absolute quantum yield determined *via* calibrated integrating sphere, excited at 380 nm. [d] Excited at 360 nm.

λ_{em} values, **1b**, **2c** and **3p**, showed a paired packing mode of *R*- and *S*-enantiomers (*RS* packing mode), and all polymorphs with longer λ_{em} values, **1c**, **2c′**, **3b** and **3c**, show an unpaired packing mode of *R*- and *S*-enantiomers (*RR*/*SS* packing mode). For instance, the *RR*/*SS* packed **1c** has an emission peak at 484 nm, being red-shifted by 50 nm compared to that of the *RS* packed **1b**.

RS packing mode

Fig. 3 depicts the *RS* paired packing of **1b**, **2c** and **3p**. The blue and yellow balls, respectively, represent the *R*- and *S*-carbon atoms. The three phenyl rings connected to the THP central ring are marked as A, B and C. As shown in Fig. 3A–C, the *R*- and *S*-enantiomers of **1b**, **2c** or **3p** are paired with each other in the *bc*-plane (front view).

The top view illustrates that the *R*- and *S*-enantiomers of **1b**, **2c** or **3p** align as two parallel lines, *R*-line and *S*-line (*R*-L and *S*-L), with opposite molecular alignment orientations (represented by two parallel blue dashed lines in Fig. 3D–F). The distances (d_1) between the ring centroids of adjacent molecules in the *R*- or *S*-lines of **1b**, **2c** and **3p** are 9.726, 9.591 and 10.677 Å, respectively (Fig. 3D–F). All molecules in **1b** are connected as a network *via* weak intermolecular hydrogen bonds (dotted bonds in Fig. 3D and S2†) (the hydrogen bond parameters are listed in Table S1†). However, no weak hydrogen bonds were found in **2c** and **3p** single crystals. The molecular packing in the unit cell and some crystallographic data of **1b**, **2c** and **3p** are shown in Fig. S2 and Table S2,† respectively.

Very interestingly, the paired enantiomers arranged as flowers with six petals (six phenyls) (Fig. 3G–I). The distances (d_2) between the ring centroids of the adjacent *R*- or *S*-enantiomers of **1b**, **2c** and **3p** are 7.067, 7.492, and 7.839 Å, respectively. The dihedral angles between adjacent phenyl ring planes (α_{dih}) and the distances between adjacent ring centroids (d_{ring}) are 37–76° and 4.294–5.308 Å, respectively (for detailed parameters see Table S1†), which indicate that short-range interactions between the six phenyls of the paired *R*- and *S*-enantiomers exist.[14] These interactions and the chiral structure of THPs are expected to be the reason for the interesting flower-like arrangement. It is worth mentioning that the short-range ring interactions in **1b** and **3p** only exist between paired *R*- and *S*-enantiomers, but the short-range ring interactions in **2c** also exist between another molecule and one of the paired *R*- and *S*-enantiomers.

RR/*SS* packing mode

Fig. 4 depicts the unpaired enantiomer packing mode (*RR*/*SS* packing mode) of **1c**, **2c′**, **3b** and **3c**. From Fig. 4A–D (front view), it can be seen that the *R*- or *S*-enantiomers of **1c**, **2c′**, **3b** or **3c** partly overlap.

The top view (only the *R*-enantiomer alignment is depicted in Fig. 4E–H) illustrates that the *R*-enantiomers of **1c**, **2c′**, **3b** or **3c** arrange in a zigzag line. The d_1 values between the ring centroids of the adjacent *R*(*S*)- and *R*(*S*)-enantiomers of **1c**, **2c′**, **3b** and **3c** are 7.53, 7.59, 7.303 (d_{1a})/7.438 (d_{1b}) and 7.754 Å, respectively, which are similar to the d_2 values but shorter than the d_1 values in the *RS* packing modes (Fig. 3). Adjacent molecules in the zigzag lines are connected *via* six, four, three and two weak hydrogen bonds for **1c**, **2c′**, **3b** and **3c**, respectively. In

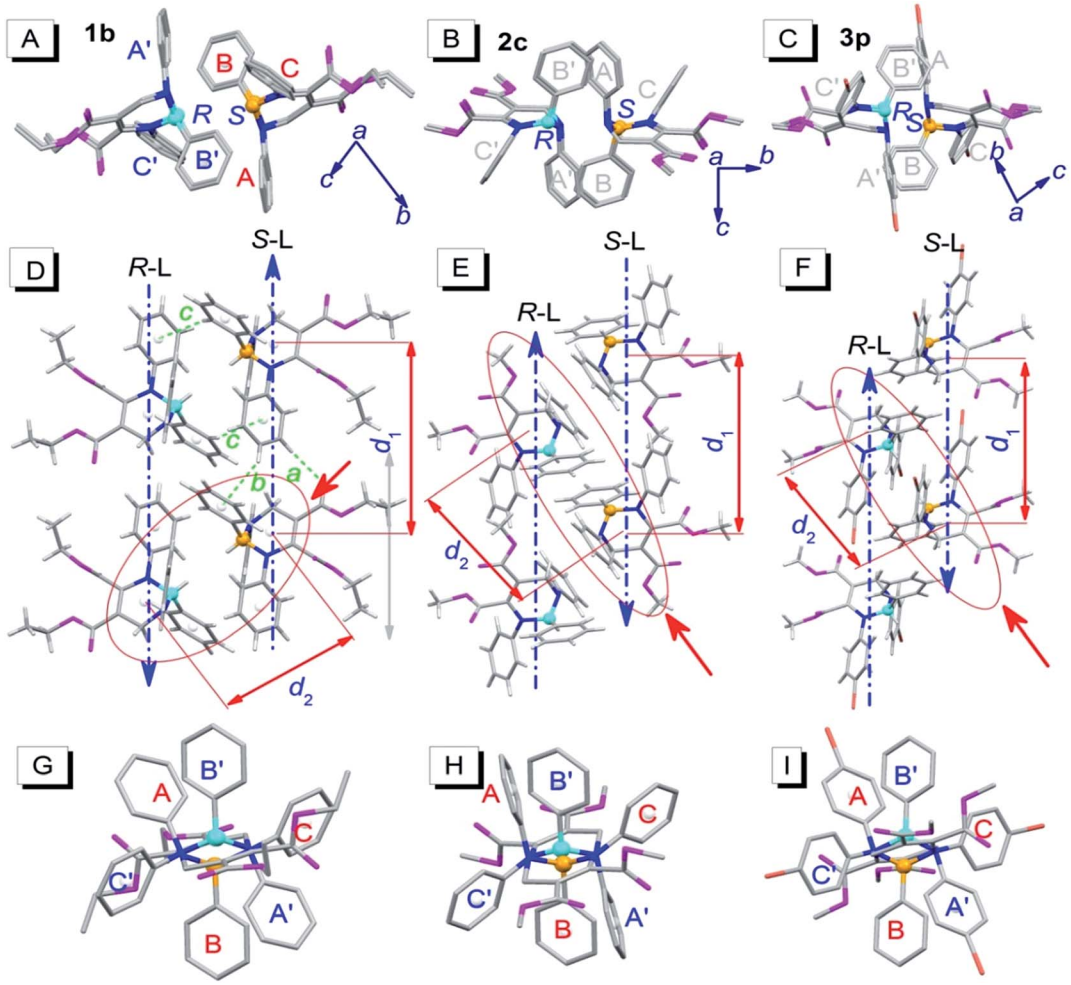

Fig. 3 Molecular packing alignments of the *R*-enantiomers (blue chiral carbon) and the *S*-enantiomers (yellow chiral carbon) of **1b** (left column), **2c** (middle column) and **3p** (right column).† (A–C) Front view; (D–F) top view; (G–I) side view from the orientation of the red solid arrow in (D–F). Weak hydrogen bonds: *a* (ary C–H···O: 2.487 Å, 177°), *b* (ary C–H···π: 2.930 Å, 146°) and *c* (ary C–H···π: 2.837 Å, 148°). Hydrogen atoms in the front and side views were omitted for clarity.

addition to the two hydrogen bonds in Fig. 4H, there are four hydrogen bonds between adjacent *R*- or *S*-enantiomers of **3c** (Fig. S3E and F†), and hence all molecules in **3c** are connected as a network *via* weak hydrogen bonds. The short-range interactions (α_{dih} = 16–69°, d_{ring} = 4.127–5.481 Å, see Table S1†) between the six phenyls of the three adjacent *R*/*S*-enantiomers are similar to those in the *RS*-packed polymorphs. The molecular stacking alignments in the unit cell of **1c**, **2c′**, **3b** and **3c** are shown in Fig. S3.† The intermolecular hydrogen bond parameters and some crystallographic data are listed in Tables S1 and S2,† respectively.

Conformations of the polymorphs of THPs 1–3

Since the molecular conformation also influences the optical properties of organic fluorophores, the conformations of these polymorphs were studied. Fig. 5 depicts the molecular conformations of the polymorphs of THP **1**. It can be seen that the conformations are stereo with phenyls A–C arranged in completely different spatial directions (up, down and in front of the central ring). There are two significant differences between the conformations of **1b** and **1c**: (a) the dihedral angle (α) between the phenyl C and the –C═C-plane in **1b** is larger than that in **1c** (Table 2); (b) the orientation of the carbonyl group at C-5 (marked by red circles) are very different. Two and one intramolecular hydrogen bonds exist in **1b** and **1c**, respectively (marked as *a* and *b*). There are intramolecular short-range ring interactions between rings A and C in **1b** and **1c** (schematically depicted in Fig. 5, and detailed data are listed in Table S1†).

The molecular conformations of other five polymorphs are shown in Fig. S4.† Polymorphs, except **2c**, with the same packing modes possess similar conformations, that is, the conformation of the *RS*-packing of **3p** is similar to that of the *RS*-packing of **1b**, and the conformations of **2c′**, **3b** and **3c** are similar to that of the *RR*/*SS*-packing of **1c**. However, the conformation of the *RS*-packed **2c** is an intermediate case between the conformations of *RS*-packed and *RR*/*SS*-packed polymorphs, that is, the α value between the phenyl C and the –C═C-plane of the *RS*-packed **2c** is similar to that of the

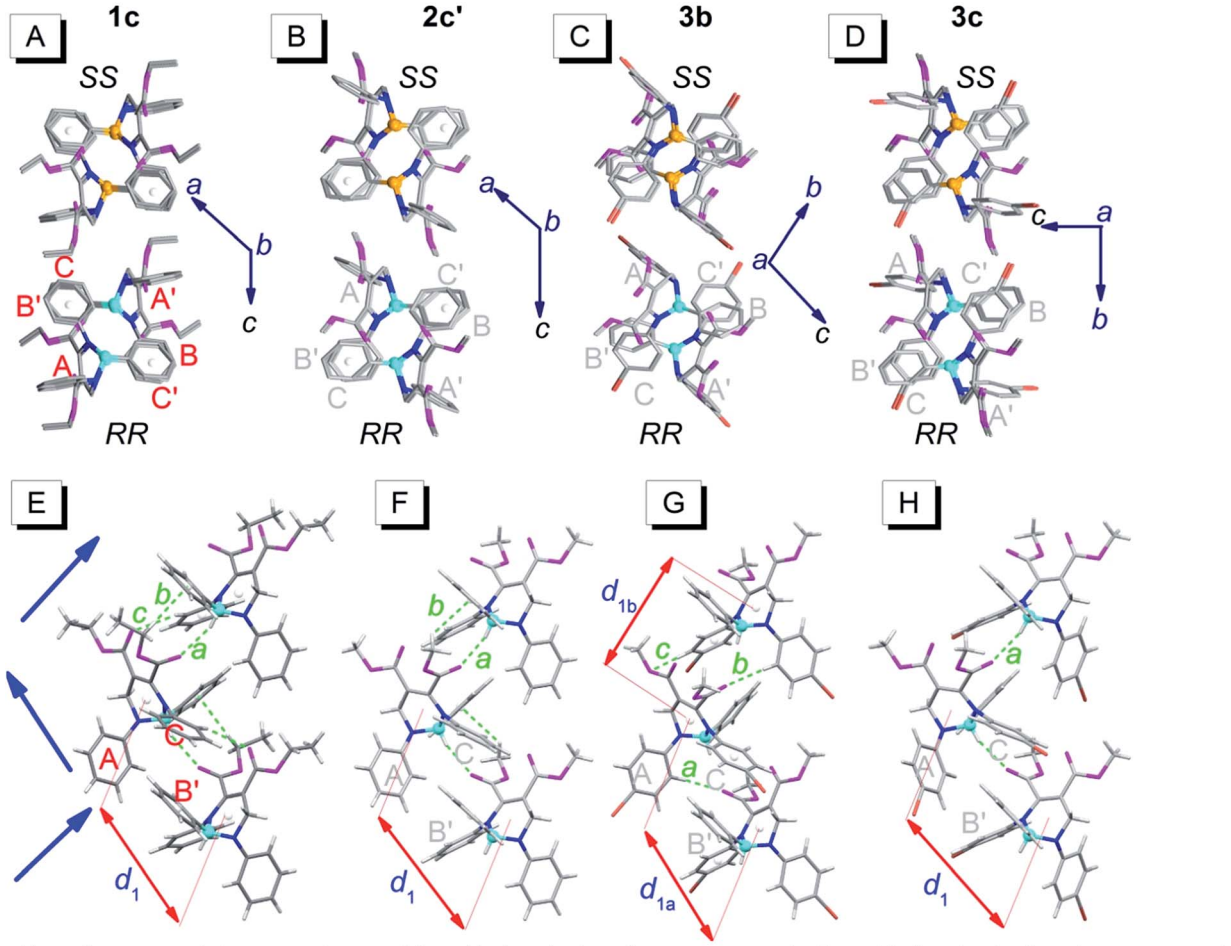

Fig. 4 Packing alignments of the *R*-enantiomers (blue chiral carbon) and the *S*-enantiomers (yellow chiral carbon) of **1c**, **2c′**, **3b** and **3c** (from left to right columns).† (A–D) Front view (hydrogen atoms were omitted for clarity); (E–H) top view. Weak hydrogen bonds: *a* (C–H···O: 2.434 Å, 143°), *b* (C–H···π: 2.634 Å, 144°) and *c* (ary C–H···O: 2.579 Å, 136°) in (E); *a* (C–H···O: 2.407 Å, 145°) and *b* (C–H···π: 2.901 Å, 124°) in (F); *a* (ary C–H···O: 2.569 Å, 176°), *b* (ary C–H···O: 2.553 Å, 165°) and *c* (ary C–H···O: 2.551 Å, 146°) in (G); *a* (C–H···O: 2.362 Å, 151°) in (H).

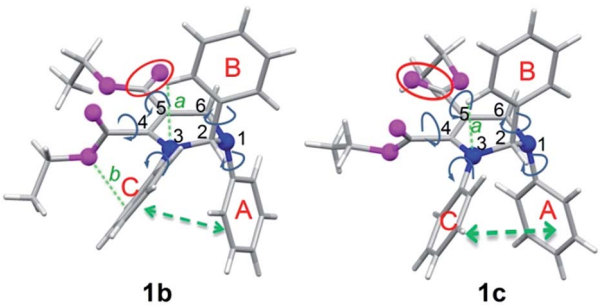

Fig. 5 Molecular conformations of polymorphs **1b** (left) and **1c** (right). Hydrogen bonds *a* (ary C–H···O: 2.505 Å, 102°), *b* (ary C–H···N: 2.578 Å, 116°) in **1b**; *a* (ary C–H···N: 2.511 Å, 102°) in **1c**.

RS-packed **1b** and **3p** (Table 2), but the orientation of the carbonyl (C=O) at C-5 is similar to that of the *RR*/*SS*-packed **1c**, **2c′**, **3b** and **3c**. It is worth mentioning that two different conformations of **3b** exist (**3b$_1$** and **3b$_2$** in Fig. S4†). The intramolecular short-range ring interactions between rings A and C in these polymorphs are shown in Table S1.†

Table 2 Some parameters related to the molecular conformations of the polymorphs of THPs **1–3**

THP	1		2		3		
Pol[a]	**1b**	**1c**	**2c**	**2c′**	**3p**	**3b**	**3c**
PM[b]	*RS*	*RR*/*SS*	*RS*	*RR*/*SS*	*RS*	*RR*/*SS*	*RR*/*SS*
λ_{em}[c]/nm	434	484	469	484	425	445	468
ΔE_1[d]/eV	2.86	2.57	2.65	2.57	2.92	2.79	2.66
α[e]/°	49.24	36.46	48.62	31.81	53.04	43.50	34.50
ΔE_2[f]/eV	4.47	4.17	4.50	4.22	4.55	4.45	4.29
λ_{bg}[f]/nm	278	298	276	295	273	279	290
λ_{ex}[g]/nm	355	409	370	387	330	365	390
$\Delta_{\lambda_{ex}-\lambda_{bg}}$/nm	77	111	94	92	57	86	100
$\Delta_{\lambda_{ab}-\lambda_{bg}}$/nm	39	19	41	22	47	41	30

[a] Pol: polymorph. [b] PM: packing mode. [c] Peak emission wavelength. [d] The energy of the peak emission wavelength. [e] Dihedral angle between phenyl C and the –C=C-plane. [f] Band gap between the HOMO and LUMO. [g] Peak excitation wavelength at lower energy area.

Theoretical calculation of HOMOs and LUMOs

To further understand the different fluorescence between these polymorphs, the highest occupied molecular orbitals (HOMOs) and the lowest unoccupied molecular orbitals (LUMOs) based on the molecular conformations of the polymorphs of THPs **1–3** were calculated. The plots of the HOMO and LUMO of **1b** and **1c** are shown in Fig. 6. The HOMO of **1b**/**1c** is mainly located on the C=C_5–C=O moiety, phenyls A and C, but the LUMO is only on two carboxylate groups and the phenyl C, which means that both a local excitation state (LE) and an intramolecular charge transfer excitation state (ICT) exist. The inter-crossed excited states are not only proved to lead to a red shift in absorption/emission but also to favor fluorescence efficiency enhancement.[15] In addition, the lone pair of electrons on N1 and the π-electrons conjugate not only through bonds but also through space[16] (marked with red circles), which can enhance electronic delocalization and restrict intramolecular motion, leading to a fluorescence efficiency enhancement and red-shifted absorption/emission to some extent. Besides the through-space conjugations marked with red circles, through-space conjugation exists between the dicarboxylates of **1c** (marked with a yellow circle), which should be one of the reasons why **1c** shows a longer wavelength emission than **1b**. The optical band gaps of **1b** and **1c** are 4.47 and 4.17 eV, respectively, which are wider than that of **1** (3.92 eV) in monomers. This demonstrates that the molecular conformations of **1** in **1b** and **1c** are more twisted than those in solutions. The plots of the HOMOs and LUMOs of the other polymorphs are similar to those of **1b** or **1c** (Fig. S5†).

AIE mechanism

The fluorescence quantum yield of an organic fluorophore depends on its radiative and non-radiative rate constants. Very high fluorescence efficiency can be realized when the k_r value is much larger than the k_{nr} value, while practically no emission will be observed when k_{nr} is much larger than k_r. Owing to intramolecular motions (the rotation of single C–C and C–N bonds and the flip of the non-aromatic central ring), the k_{nr} values of THPs **1–3** in solution are expected to be very large like those of other AIE compounds.[17] In addition, THPs **1–3** have low conjugated molecular structures, that is, very small k_r values. Therefore, THPs **1–3** show practically no emission in solution.

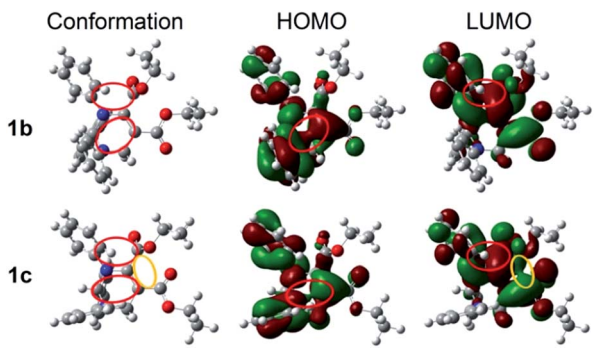

Fig. 6 Molecular conformations, HOMOs and LUMOs of polymorphs **1b** and **1c**.

However, upon aggregation, the k_{nr} values of THPs **1–3** dramatically decrease to 0.05–3.48 × 10^8 s^{-1} because of the restriction of intramolecular motion (RIM) by intra- and intermolecular interactions, and their k_r values increase to 0.41–1.03 × 10^8 s^{-1}, which are as large as those of conventional π-conjugated fluorophores,[18] owing to the improved electronic coupling *via* through-bond and through-space pathways (Fig. 6 and S5†) as well as the inter-crossed radiative-favorable LE and ICT processes. Consequently, THPs **1–3** show a strong AIE effect and the polymorphs emit intense fluorescence. By comparing the k_r and k_{nr} values of the polymorphs of THPs **1–3** and the factors influencing these values, it can be deduced that: (a) *RS*-packing should be more favourable for a radiative process than *RR*/*SS*-packing because the k_r values of the *RS*-packing polymorphs are slightly higher than those of their corresponding *RR*/*SS*-packing polymorphs even though the *RS*-packing conformations are more twisted and do not contain through-space conjugation between the dicarboxylates. This might arise from the flower-like packing alignment between *R*- and *S*-enantiomers (Fig. 3G–I) because this special packing alignment is similar to the reported cross-stacking mode with a high fluorescence efficiency.[19] (b) The differences in Φ_F between these polymorphs should mainly result from the different extents of RIM, that is, different k_{nr} values, because they possess the same molecular structure and have similar k_r values. The short-range interaction between the intramolecular phenyls A and C may be crucial in decreasing the k_{nr} value of these polymorphs, as the distances between the intramolecular phenyls A and C in all polymorphs with the lowest k_{nr} value (**1c**, **2c** and **3c**) are shorter than those of their corresponding polymorphs (Table S1†).

The red-shifted absorption and emission spectra of organic fluorophores in aggregates are mainly caused by the planarization of its π-conjugated moiety, intramolecular and intermolecular interactions. The planarization and intramolecular interactions depend on the molecular conformation, but intermolecular interactions depend on the molecular stacking mode. To evaluate the influences of the conformation and the packing mode of the polymorphs of THPs **1–3** on their absorption wavelengths, the lowest energy excitation peaks λ_{ex} of these polymorphs and the band gap values (λ_{bg}) between their HOMOs and LUMOs and their differences ($\Delta_{\lambda_{ex}-\lambda_{bg}}$) have been listed in Table 2. The differences ($\Delta_{\lambda_{ab}-\lambda_{bg}}$) between the lowest energy absorption peaks (λ_{ab}) of THPs **1–3** in solution and the λ_{bg} values are also listed in Table 2. The influence of molecular conformation/stacking mode on the absorption spectra of these polymorphs can be evaluated by the $\Delta_{\lambda_{ab}-\lambda_{bg}}$/$\Delta_{\lambda_{ex}-\lambda_{bg}}$ values. It can be see that the molecular packing modes in these polymorphs can lead to a 57–111 nm ($\Delta_{\lambda_{ex}-\lambda_{bg}}$) red-shift in their excitation spectra, but their twisted conformation leads to a 19–47 nm ($\Delta_{\lambda_{ab}-\lambda_{bg}}$) blue-shift. Therefore, the large red-shifts in the absorption and emission spectra of these polymorphs are mainly attributed to intermolecular ring interactions. This is because the ring interactions of adjacent π-conjugated molecules have been demonstrated to cause a larger, non-structural red-shift in the absorption/emission spectra compared to that caused by molecular planarization.[20]

Then, what is the reason for the differences in the $\Delta_{\lambda_{ex}-\lambda_{bg}}$ and $\Delta_{\lambda_{ab}-\lambda_{bg}}$ values between the polymorphs of THPs **1–3**? By comparing the $\Delta_{\lambda_{ex}-\lambda_{bg}}$ values of these polymorphs and the intermolecular interactions in these polymorphs, it can be deduced that the $\Delta_{\lambda_{ex}-\lambda_{bg}}$ values should mainly depend on the short-range (4.1–5.5 Å) interactions between the phenyls of adjacent molecules (the short-range ring interactions in **1c**, **1b**, **2c**, **2c′**, **3p**, **3b** and **3c** are depicted in Fig. S6†). Short-range ring interactions in the *RR*/*SS*-packing polymorphs **1c** and **3c** exist among all zigzag-aligned *R*- or *S*-enantiomers (Fig. 4E–H), but those in their corresponding *RS*-packing polymorphs **1b** and **3p** only exist between two paired *R*- and *S*-enantiomers. Therefore, the former can lead to a larger electron delocalization than the latter, and hence the $\Delta_{\lambda_{ex}-\lambda_{bg}}$ values (110 and 100 nm) of the *RR*/*SS*-packing polymorphs **1c** and **3c** are much larger than those (77 and 57 nm) of their corresponding polymorphs **1b** and **3p**. Although **2c** also formed a *RS*-packing mode, the short-range ring interactions in it are not limited to two paired *R*- and *S*-enantiomers (Fig. S6†) and are similar to those in its *RR*/*SS*-packing polymorph **2c′**, and hence *RS*-packing **2c** and *RR*/*SS*-packing **2c′** possess similar $\Delta_{\lambda_{ex}-\lambda_{bg}}$ values (94 and 92 nm). By comparing the $\Delta_{\lambda_{ab}-\lambda_{bg}}$ values of these polymorphs and their conformations, it can be deduced that the differences in the $\Delta_{\lambda_{ab}-\lambda_{bg}}$ values between these polymorphs should mainly be caused by the different dihedral angle α between the phenyl C and the –C═C-plane (Table 2) and by the conjugation between the dicarboxylates (with or without through-space conjugation in Fig. 6 and S5†). For example, the $\Delta_{\lambda_{ab}-\lambda_{bg}}$ value of **3b** is 6 nm smaller than that of **3p** but 11 nm larger than that of **3c**, even though the differences in the dihedral angle α between **3b** and **3p** and between **3b** and **3c** are similar (9.54 and 9.00°). The reason for this should be that the difference in the $\Delta_{\lambda_{ab}-\lambda_{bg}}$ value between **3b** and **3p** is mainly caused by their different α values but the difference in the $\Delta_{\lambda_{ab}-\lambda_{bg}}$ value between **3b** and **3c** arises from their different α values and from conjugation between the dicarboxylates (Fig. S5†).

Conclusions

We have prepared seven polymorphs using the racemic THPs **1–3**, and studied the influence of their molecular packing mode and conformation on their optical properties. The experimental results indicate that the polymorphs with the shortest λ_{ex} and λ_{em} values possess a *RS*-packing mode and a more twisted conformation without through-space conjugation between the dicarboxylates, but the polymorphs with longer λ_{ex} and λ_{em} values adopt *RR*/*SS*-packing modes with through-space conjugation between the dicarboxylates. The conformations of these polymorphs are stereo and more twisted than those of their monomers. Although THPs **1–3** show practically no emission in solution owing to their low conjugated molecular structures and high intramolecular motions, they can form emissive polymorphs by through-bond and through-space electron coupling in aggregates. These new fluorophores with unique molecular structures, easily-controllable packing modes of the *R*- and *S*-enantiomers, and strong AIE effects are expected to be very useful for practical and theoretical research as well as the design of new highly emissive fluorophores with AIE properties.

Acknowledgements

We thank Ian D. Williams and Herman H. Y. Sung for support on the collection and analysis of some XRD data, we thank Zheng S. C. and Yang W. J. for measurement of the optical spectra, and we thank Huang L. for the preparation of two polymorphs. This work was supported by the National Natural Science Foundation of China (21272111 and 31370781), the National Basic Research Program of China (973 Program; 2013CB834701), the Research Grants Council of Hong Kong (604711, 604913, HKUST2/CRF/10 and N_HKUST620/11), Innovation and Technology Commission (ITCPD/17-9), and the University Grants Committee of Hong Kong (AoE/P-03/08).

Notes and references

1 (*a*) S. Reineke, F. Lindner, G. Schwartz, N. Seidler, K. Walzer, B. Lussem and K. Leo, *Nature*, 2009, **459**, 234–238; (*b*) K. H. Lee, Y. S. Kwon, J. Y. Lee, S. Kang, K. S. Yook, S. O. Jeon, J. Y. Lee and S. S. Yoon, *Chem.–Eur. J.*, 2011, **17**, 12994–13006; (*c*) L. Yao, S. Zhang, R. Wang, W. Li, F. Shen, B. Yang and Y. Ma, *Angew. Chem.*, 2014, **126**, 2151–2155.

2 (*a*) Y. S. Zhao, A. Peng, H. Fu, Y. Ma and J. Yao, *Adv. Mater.*, 2008, **20**, 1661–1665; (*b*) Y. S. Zhao, J. Xu, A. Peng, H. Fu, Y. Ma, L. Jiang and J. Yao, *Angew. Chem. Int. Ed.*, 2008, **47**, 7301–7305; (*c*) X. Gu, J. Yao, G. Zhang, Y. Yan, C. Zhang, Q. Peng, Q. Liao, Y. Wu, Z. Xu and Y. Zhao, *Adv. Funct. Mater.*, 2012, **22**, 4862–4872.

3 S. A. Jenekhe and J. A. Osaheni, *Science*, 1994, **265**, 765–768.

4 J. Luo, Z. Xie, J. W. Lam, L. Cheng, H. Chen, C. Qiu, H. S. Kwok, X. Zhan, Y. Liu, D. Zhu and B. Z. Tang, *Chem. Commun.*, 2001, 1740–1741.

5 (*a*) W. Z. Yuan, Y. Gong, S. Chen, X. Y. Shen, J. W. Lam, P. Lu, Y. Lu, Z. Wang, R. Hu and N. Xie, *Chem. Mater.*, 2012, **24**, 1518–1528; (*b*) J. Huang, N. Sun, P. Chen, R. Tang, Q. Li, D. Ma and Z. Li, *Chem. Commun.*, 2014, **50**, 2136–2138.

6 (*a*) Y. Liu, Y. Yu, J. W. Y. Lam, Y. Hong, M. Faisal, W. Z. Yuan and B. Z. Tang, *Chem.–Eur. J.*, 2010, **16**, 8433–8438; (*b*) M. Wang, G. Zhang, D. Zhang, D. Zhu and B. Z. Tang, *J. Mater. Chem.*, 2010, **20**, 1858–1867; (*c*) Y. Liu, C. Deng, L. Tang, A. Qin, R. Hu, J. Z. Sun and B. Z. Tang, *J. Am. Chem. Soc.*, 2011, **133**, 660–663; (*d*) X. Li, K. Ma, S. Zhu, S. Yao, Z. Liu, B. Xu, B. Yang and W. Tian, *Anal. Chem.*, 2013, **86**, 298–303; (*e*) Z. Song, Y. Hong, R. T. K. Kwok, J. W. Y. Lam, B. Liu and B. Z. Tang, *J. Mater. Chem. B*, 2014, **2**, 1717–1723.

7 (*a*) Z. Zhao, J. W. Lam, C. Y. Chan, S. Chen, J. Liu, P. Lu, M. Rodriguez, J. L. Maldonado, G. Ramos-Ortiz, H. H. Sung, I. D. Williams, H. Su, K. S. Wong, Y. Ma, H. S. Kwok, H. Qiu and B. Z. Tang, *Adv. Mater.*, 2011, **23**, 5430–5435; (*b*) R. Hu, J. W. Y. Lam, Y. Liu, X. Zhang and B. Z. Tang, *Chem.–Eur. J.*, 2013, **19**, 5617–5624.

8 B.-K. An, S.-K. Kwon, S.-D. Jung and S. Y. Park, *J. Am. Chem. Soc.*, 2002, **124**, 14410–14415.

9 X. Fan, J. Sun, F. Wang, Z. Chu, P. Wang, Y. Dong, R. Hu, B. Z. Tang and D. Zou, *Chem. Commun.*, 2008, 2989–2991.
10 (*a*) Y. Hong, J. W. Lam and B. Z. Tang, *Chem. Soc. Rev.*, 2011, **40**, 5361–5388; (*b*) T. Nicolini, A. Famulari, T. Gatti, J. Martí-Rujas, F. Villafiorita-Monteleone, E. V. Canesi, F. Meinardi, C. Botta, E. Parisini, S. V. Meille and C. Bertarelli, *J. Phys. Chem. Lett.*, 2014, **5**, 2171–2176.
11 Q. Zhu, L. Huang, Z. Chen, S. Zheng, L. Lv, Z. Zhu, D. Cao, H. Jiang and S. Liu, *Chem.–Eur. J.*, 2013, **19**, 1268–1280.
12 L. Huang, J. Su, D. Zhong, H. Wang, R. Liu, L. Yu, Q. Zhu and S. Liu, *RSC Adv.*, 2013, **3**, 13286–13292.
13 Q. Zhu, L. Huang, J. Su and S. Liu, *Chem. Commun.*, 2014, **50**, 1107–1109.
14 G. D. Scholes and K. P. Ghiggino, *J. Phys. Chem.*, 1994, **98**, 4580–4590.
15 W. Li, D. Liu, F. Shen, D. Ma, Z. Wang, T. Feng, Y. Xu, B. Yang and Y. Ma, *Adv. Funct. Mater.*, 2012, **22**, 2797–2803.
16 Z.-L. Gong, Y.-W. Zhong and J. Yao, *Chem.–Eur. J.*, 2015, **21**, 1554–1566.
17 (*a*) J. Chen, C. C. W. Law, J. W. Y. Lam, Y. Dong, S. M. F. Lo, I. D. Williams, D. Zhu and B. Z. Tang, *Chem. Mater.*, 2003, **15**, 1535–1546; (*b*) G. Yu, S. Yin, Y. Liu, J. Chen, X. Xu, X. Sun, D. Ma, X. Zhan, Q. Peng, Z. Shuai, B. Tang, D. Zhu, W. Fang and Y. Luo, *J. Am. Chem. Soc.*, 2005, **127**, 6335–6346.
18 (*a*) S. Choi, J. Bouffard and Y. Kim, *Chem. Sci.*, 2014, **5**, 751–755; (*b*) S. Yagai, S. Okamura, Y. Nakano, M. Yamauchi, K. Kishikawa, T. Karatsu, A. Kitamura, A. Ueno, D. Kuzuhara, H. Yamada, T. Seki and H. Ito, *Nat. Commun.*, 2014, **5**, 1–10.
19 (*a*) Z. Xie, B. Yang, F. Li, G. Cheng, L. Liu, G. Yang, H. Xu, L. Ye, M. Hanif, S. Liu, D. Ma and Y. Ma, *J. Am. Chem. Soc.*, 2005, **127**, 14152–14153; (*b*) C.-H. Zhao, A. Wakamiya, Y. Inukai and S. Yamaguchi, *J. Am. Chem. Soc.*, 2006, **128**, 15934–15935.
20 M. Levitus, K. Schmieder, H. Ricks, K. D. Shimizu, U. H. F. Bunz and M. A. Garcia-Garibay, *J. Am. Chem. Soc.*, 2001, **123**, 4259–4265.